Supplemental Information

Nonlinear Dynamics Underlying Sensory Processing Dysfunction in Schizophrenia

Claudia Lainscsek[1,2], Aaron L. Sampson[1,3], Robert Kim[1,3], Michael L. Thomas[7,8], Karen Man[1,4], Xenia Lainscsek[5], The COGS Investigators, Neal R. Swerdlow[7], David L. Braff[6,7], Terrence J. Sejnowski[1,2,9], Gregory A. Light[6,7]

[1] Computational Neurobiology Laboratory, Salk Institute for Biological Studies, La Jolla, CA, USA
[2] Institute for Neural Computation, University of California San Diego, La Jolla, CA
[3] Neurosciences Graduate Program, University of California San Diego, La Jolla, CA
[4] New Jersey Medical School, 185 South Orange Avenue, Newark, NJ
[5] Technische Universitt Graz, 8010 Graz; Austria
[6] Veterans Integrated Service Network - 22 Mental Illness, Research, Education and Clinical Center (MIRECC), Veterans Affairs San Diego Healthcare System, San Diego, CA 92161
[7] Department of Psychiatry, University of California San Diego, La Jolla, CA
[8] Department of Psychology, Colorado State University, Fort Collins, CO
[9] Division of Biological Sciences, University of California San Diego, La Jolla, CA

www.pnas.org/cgi/doi/10.1073/pnas.1810572116

1 Embeddings

Delay Differential Analysis (DDA) is a functional embedding technique that employs delay differential equations (DDEs) to provide a highly specific and low-dimensional representation of an observable time series. Even without direct access to all the system state variables, DDEs can provide a small subset of features that capture the relevant dynamics of a system [1–5]. DDEs combine two different types of embedding: a delay embedding and a derivative embedding. An embedding refers to the mapping of a single time series into a multidimensional object [6–9]. A delay embedding maps a single time series $x(t)$ into a multidimensional space spanned by $x(t)$ and its delayed versions $x(t-\tau_n)$, where the delays τ_n are positive integers. Similarly, a derivative embedding maps $x(t)$ into a higher dimensional space constructed by $x(t)$ and its n-order derivatives. Both types of embedding, delay and derivative embedding, are diffeomorph to the original unknown dynamical system. DDA combines the two types of embedding by relating them in a polynomial function to extract relevant dynamical information from a single time series. For simplicity, Eq. (1) shows a DDE with a first-order derivative embedding and a delay embedding:

$$\dot{x} = \sum_{i=1}^{I} a_i \prod_{n=1}^{N} x_{\tau_n}^{m_{n,i}} \tag{1}$$

Here, $\tau_n, m_{n,i}, I \in \mathbb{N}_0$, $x = x(t)$, and $x_{\tau_n} = x(t-\tau_n)$.

In order to illustrate the relationship between a dynamical system and its DDA features (the coefficients a_i and the delays τ_n) we discuss the following simple example. Consider a second-order linear differential equation defined by:

$$\ddot{x} = a\,x \tag{2}$$

Eq. (2) is then equivalent to the following dynamical system:

$$\begin{aligned} \frac{dx}{dt} &= y \\ \frac{dy}{dt} &= a\,x \end{aligned} \tag{3}$$

The above dynamical system has the special solution:

$$\begin{aligned} x &= cos(\omega t) \\ a &= -\omega^2\,. \end{aligned} \tag{4}$$

Therefore, it is easy to see that Eq. (3) is the functional form of the derivative embedding of $x(t) = cos(\omega t)$. Both $x(t)$ and $y(t)$ can be solved by numerically integrating Eq. (3), and the phase space plot of x and $\frac{y}{\omega}$ can be plotted as shown in Supplementary Fig. 1.

If only $x(t)$ is available, the phase space spanned by $x(t)$ and $y(t)$ can be still constructed using an embedding. In Supplementary Fig. 2, two embeddings of the time series from Supplementary Fig. 1 are shown–a delay embedding and a differential embedding. Since an

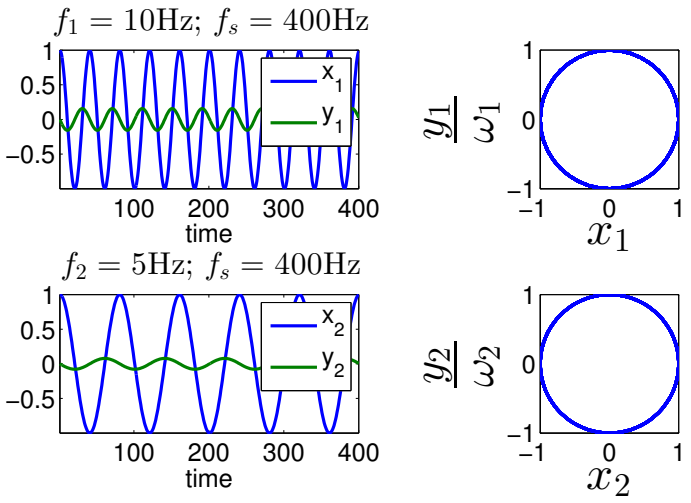

Supplementary Figure 1. The left plots show the numerically integrated $x(t)$ and $y(t)$ in Eq. (3). The same integration constant dt was used for both plots. Only the parameter a was different according to the sampling rates $f_1 = 10$ Hz for the upper plots and $f_2 = 5$ Hz for the lower plots. On the right plots the phase plots are shown. The y axes are scaled by ω to obtain a circle.

ellipse is topologically equivalent to a circle, both types of embeddings recover the structure of the original phase space (compare the right plots in Supplementary Fig. 1 with Supplementary Fig. 2).

For the above example, the simplest linear delay differential equation (DDE) is

$$\dot{x} = b\, x_\tau \tag{5}$$

with $x_\tau = x(t-\tau)$. Again the special solution here is $x(t) = cos(\omega t)$ [3, 10]

$$\begin{aligned} -\omega sin(\omega t) &= b\, cos(\omega t - \tau) \\ b &= (-1)^n \omega \\ \tau &= \frac{\pi(2n-1)}{2\omega} \end{aligned} \tag{6}$$

where b is proportional to the frequency ω, and τ is inversely proportional to the frequency ω. DDA is therefore able to recover the systems parameters of the dynamical system. More examples including non-linear dynamical systems and the structure of the parameter space can be found in [11, 12].

For a more complex dynamical system, relating the derivative and delay embeddings could provide additional information regarding the underlying dynamical system. This is the principal idea behind DDA: a derivative embedding is matched to a polynomial function of delay embeddings to uncover dynamical information.

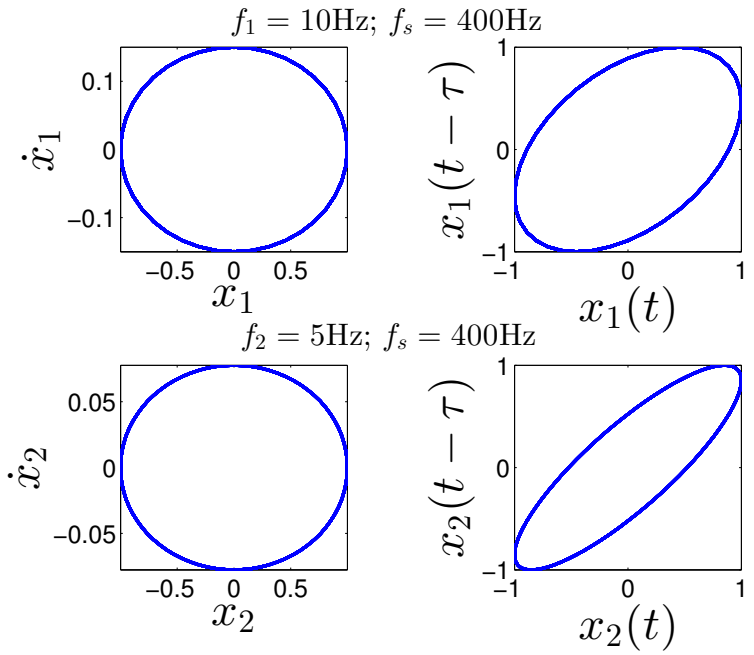

Supplementary Figure 2. Derivative (left) and delay (right) embeddings for the time series $x(t)$ of the numerically integrated Eq. (3).

2 DDA details

For the derivative embedding, the first-order derivative is numerically estimated by using a weighted center derivative [13]

$$\dot{x} = \frac{1}{N}\sum_{n=1}^{N}\frac{x(t-n) - x(t+n)}{2n}\,, \tag{7}$$

where N is the number of forward and backwards steps in computing the derivative. Here we use $N = 10$ δt, where $\delta t = \frac{1}{fs}$ and f_s is the sampling rate ($f_s = 1000$ Hz).

The least square mean error, used as one of the features in DDA, is computed according to:

$$\rho = \sqrt{\frac{1}{K}\sum_{k=1}^{K}\left(\dot{x}_{t_k} - \sum_{i=1}^{I} a_i \prod_{n=1}^{N} x_{t_k,\tau_n}^{m_{n,i}}\right)^2} \tag{8}$$

for K data points, where $\dot{x}_{t_k} = \dot{x}(t_k)$ and $x_{t_k,\tau_n} = x(t_k - \tau_n)$.

2.1 Cross-trial DDA

Cross-trial DDA is illustrated in Supplementary Fig. 3. In this approach, data from equivalent time windows in multiple trials is combined to compute cross-trial DDA features. A key

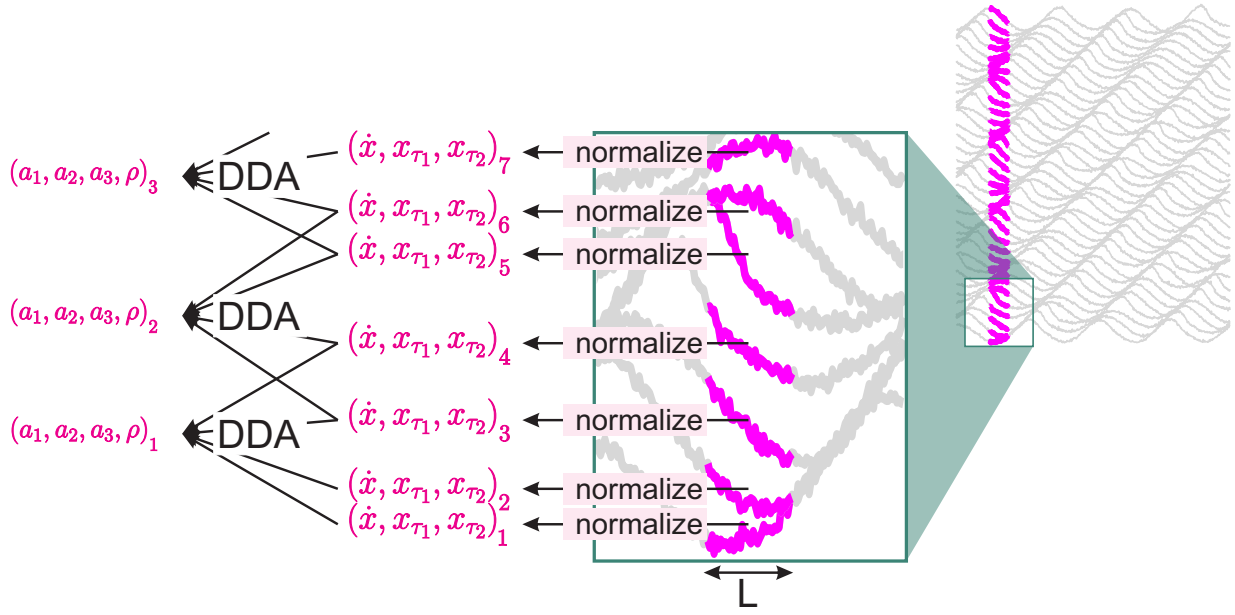

Supplementary Figure 3. Cross-trial DDA: In this example, data from sets of 4 trials are combined assuming ergodicity [14]. L is the temporal window length (see also Fig. 2). The data from each time window and trial are normalized to zero mean and unit variance and then combined to compute the DDA features simultaneously.

advantage of this approach is that it allows shorter time windows to be used. Additionally, it can serve as a test of dynamical coherence across trials.

In Supplementary Fig. 4(a) the data show dynamical incoherence. This means each trial covers a small and different part of the embedding. In Supplementary Fig. 4(b) the data are dynamically coherent and therefore the same part of the embedding is covered in each trial. There should be a much bigger difference between single-trial and cross-trial DDA in the case of dynamical incoherence (as in Supplementary Fig. 4(a)). This is because in the case of dynamical incoherence, the short data windows do not sample enough of the embedding to efficiently estimate the coefficients and the variance of the coefficients for all trials will be large. Therefore, mean features computed across the individual channels will be very different from the cross-trial features, where despite the small data window a large part of the embedding is covered. For the case of dynamical coherence, both versions give similar results. In [5] the same concept was introduced for spectral analysis.

2.2 Structure selection

2.2.1 Supervised structure selection

Supplementary Fig. 5 illustrates how the DDE model that best distinguishes NCS subjects from SZ patients was selected.

To obtain an equal amount of data for each subject, the first 150 deviant trials were used.

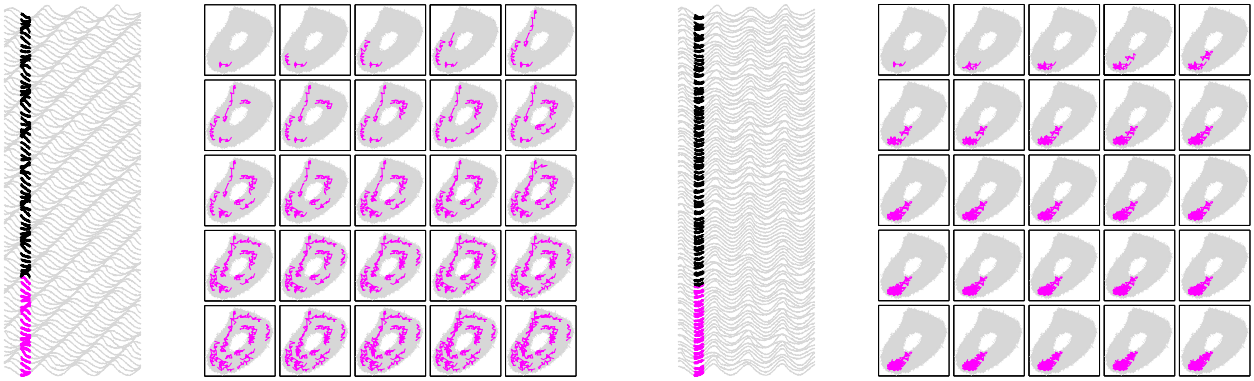

(a) dynamical incoherence (b) dynamical coherence

Supplementary Figure 4. Cross-trial DDA coverage of the embedding space.

The raw EEG data from these 150 trials were first normalized to zero mean and unit variance to disregard amplitude information. Then the DDA features were extracted from 50 ms time windows ($L = 50\delta t$) with a time shift of 5 ms (resulting in 74 temporal windows from trials of 450 ms) either single- or cross-trial. We combined 40 trials for the cross-trial DDA (in Supplementary Fig. 3 the example of 4 trials is shown) and shifted the cross-trial windows by 10 trials (in Supplementary Fig. 3 the example of 2 trials is shown). This resulted in 12 trial windows across the 150 trials for each temporal window (see Fig. 3).

Next, repeated random subsampling cross-validation (CV) [15] was carried out: the data are divided into training data (5 from each group) and testing data (remaining 1620 subjects) 20000 times (see Supplementary Fig. 5). This process is carried out for each of seven three-term DDEs that have been shown to be discriminative EEG models,

$$\begin{aligned}
\text{Model \#1:} \quad \dot{x} &= a_1 x_1 + a_2 x_2 + a_3 x_1^2 \\
\text{Model \#2:} \quad \dot{x} &= a_1 x_1 + a_2 x_2 + a_3 x_1 x_2 \\
\text{Model \#3:} \quad \dot{x} &= a_1 x_1 + a_2 x_2 + a_3 x_1^3 \\
\text{Model \#4:} \quad \dot{x} &= a_1 x_1 + a_2 x_2 + a_3 x_1^2 x_2 \\
\text{Model \#5:} \quad \dot{x} &= a_1 x_1 + a_2 x_2 + a_3 x_1^4 \\
\text{Model \#6:} \quad \dot{x} &= a_1 x_1 + a_2 x_2 + a_3 x_1^3 x_2 \\
\text{Model \#7:} \quad \dot{x} &= a_1 x_1 + a_2 x_2 + a_3 x_1^2 x_2^2
\end{aligned} \tag{9}$$

with $x_n = x(t - \tau_n)$. For each of these models all possible delay combinations for τ_1 and τ_2 between $1\delta t$ and $15\delta t$ are run through the CV. This is done for each of the 74 temporal windows separately. We trained on only 5 subjects in each group to show that 1) if "typical" subjects are selected for training, a low number should be enough for training, 2) if "atypical" subjects are selected for training, the classification/results can be opposite 3) the ratio of "typical" to "atypical" subjects sets the maximum performance possible by using the mean weights of the CV. Here we have a big data set of 1640 subjects. This is not the case for many studies. We therefore want to use the beforementioned properties of our CV to dynamically cluster the data and separate "typical" subjects from "atypical" ones. This dynamic clustering technique is a topic of its own and will be published separately.

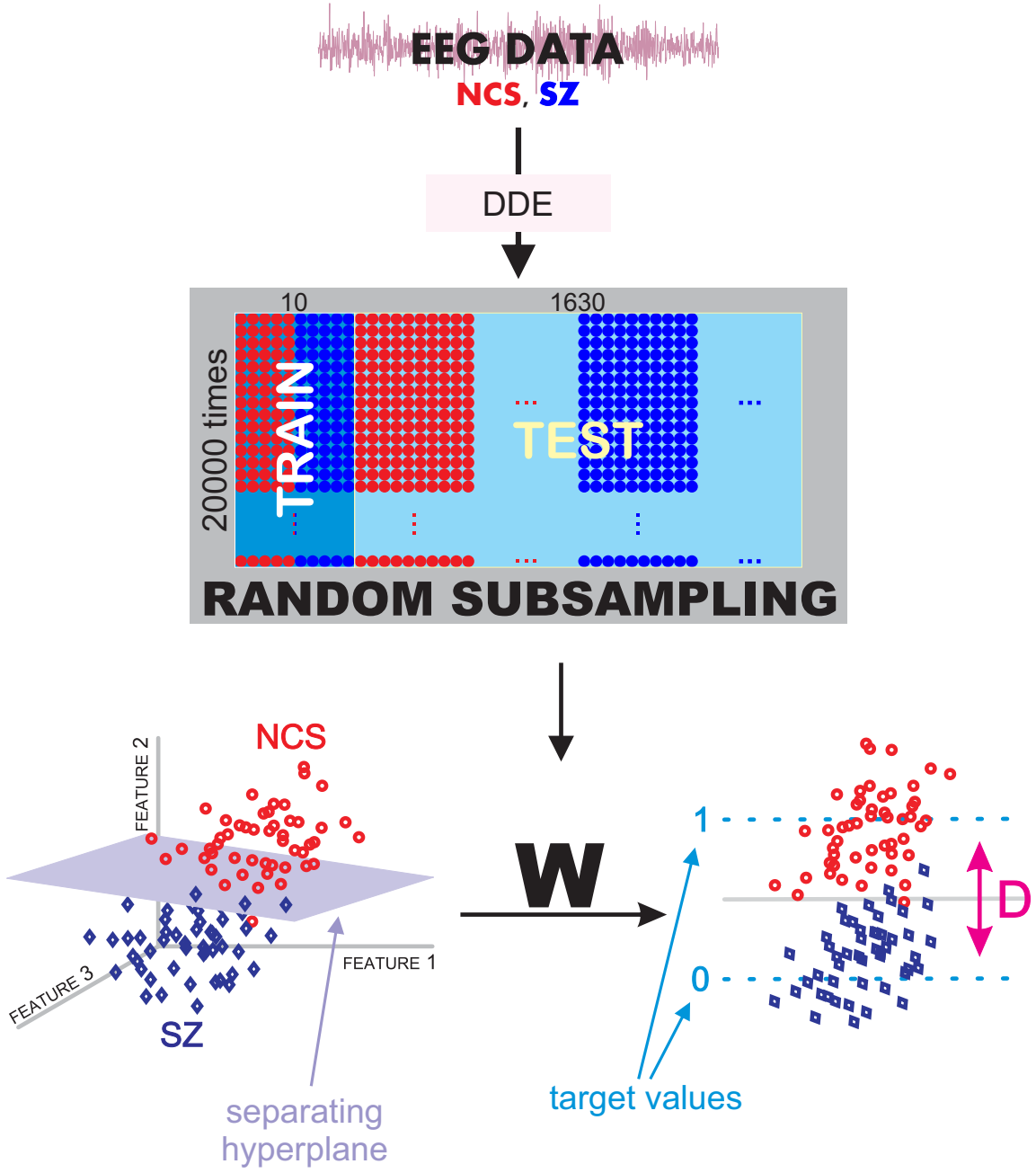

Supplementary Figure 5. Random subsampling cross-validation and construction of the weight matrix.

The performance of the DDA classification was evaluated by computing the area under the ROC curve, A'. In this case, the ROC curve was a plot of the cumulative distribution function of the NCS subject group versus that of the SZ subject group. To calculate the area, the distances from the hyperplane D were ranked from the greatest positive value to

the greatest negative value, and the A' approximated as follows [16]:

$$A' = \frac{S_0 - \frac{n_0(n_0+1)}{2}}{n_0 n_1} \tag{10}$$

where S_0 is the sum of the ranks of the NCS subject classifications, n_0 is the number of NCS subjects, and n_1 is the number of SZ subjects.

Supplementary Figs. 6 and 7 show the distributions of the best DDE model forms and the best delays for each of the 74 temporal windows.

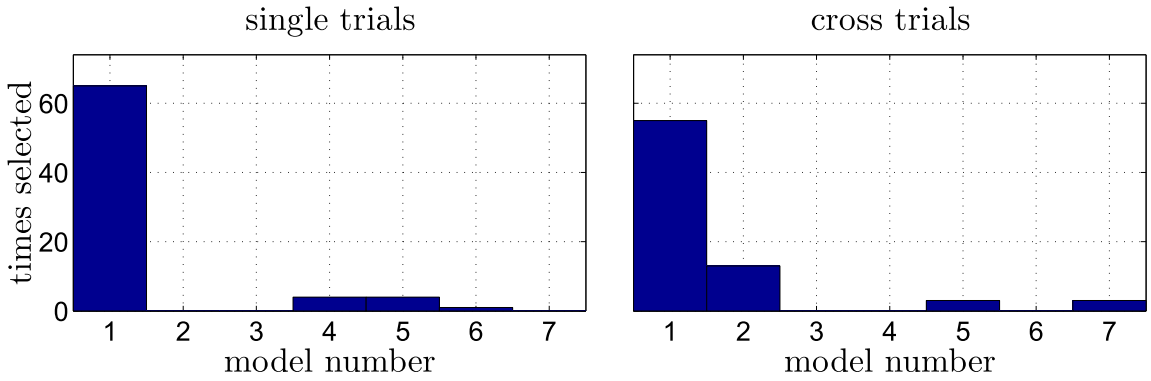

Supplementary Figure 6. Models selected for each of the 74 time windows.

Model #1 was the most often selected model for both approaches (Supplementary Fig. 6). This makes sense since all the data came from the same dynamical system and therefore the model structure should be consistent across the data. This model was used for the analyses presented in the main paper. The delays selected across the time windows (Supplementary Fig. 7)

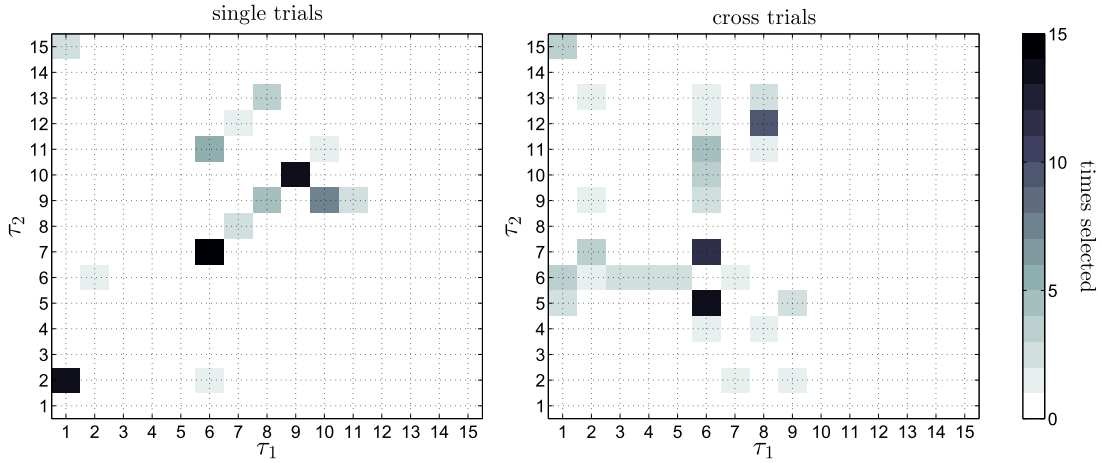

Supplementary Figure 7. Delay pairs selected for each of the 74 time windows using supervised structure selection for model #1 (11).

were different for the single- and cross-trial approach. This could point to differences in the cross-trial dynamical coherence across the temporal windows and will be a topic of further

investigation. In this paper, we chose the best performing delay pair for each temporal data window to account for the changes in the nonlinear cocktail of dominant time-scales throughout the trials.

2.2.2 Unsupervised structure selection

In an unsupervised approach, the model selected as best representing the dataset is the one which generated the minimum error ρ. The analysis was again done in both the single- and cross-trial approaches and for each temporal window separately. The only model used was

$$\dot{x} = a_1 x_1 + a_2 x_2 + a_3 x_1^2 \tag{11}$$

and the best delays were very consistent across the trials. The best delays were $\tau = (9, 3)\ \delta t$ for the single-trial approach and $\tau = (3, 8)\ \delta t$ for the cross-trial approach for most of the windows (see Supplementary Fig. 8).

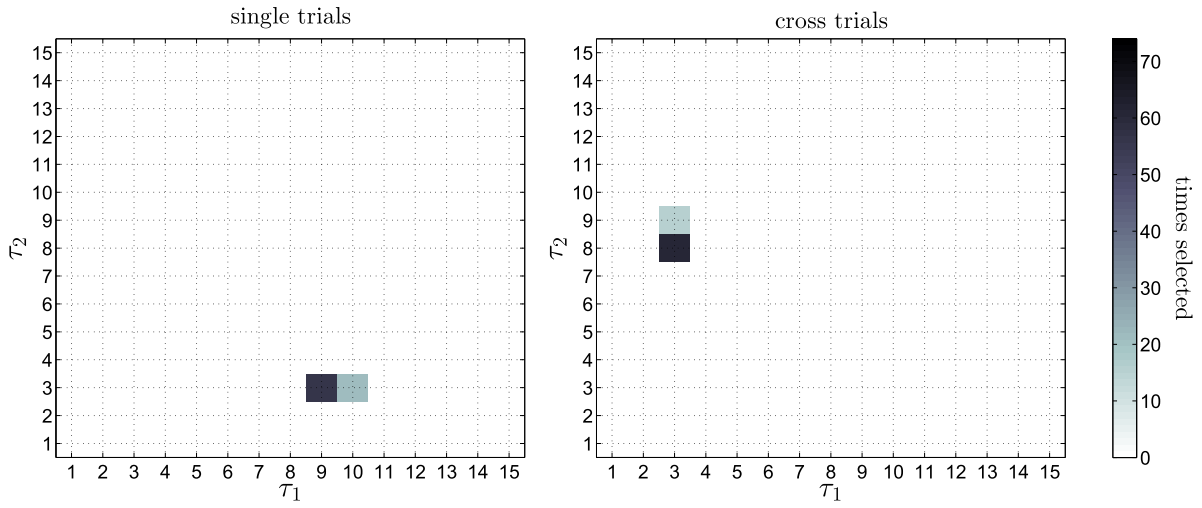

Supplementary Figure 8. Delay pairs selected for each of the 74 time windows using unsupervised structure selection for model #1 (11).

3 COGS-2 Clinical and Demographical Characteristics

COGS-2 included 1790 (966 SZ subjects and 824 NCS subjects) participants tested at the five COGS-2 test sites: University of California San Diego, University of California Los Angeles, University of Washington, University of Pennsylvania, and Mount Sinai School of Medicine. ERP data were collected from all 1790 participants, but 91% of the participants (SZ $n = 877$, NCS $n = 753$) had data with sufficient quality (as determined by signal-to-noise ratio) to permit further analysis. As noted in our previous publication ([17]), the reason for data loss primarily included correctable errors in administration (e.g., failing to plug the electrodes into the correct port on the analog amplifiers, and failing to pause the recording

due to poor signal quality, including excessive muscle artifact resulting in most trials being excluded using the automated artifact rejection procedures).

The clinical and demographic characteristics of the participants are shown in Supplementary Table 1 (adapted from [17]).The diagnostic criteria were established by a modified version of the Structural Clinical Interview for DSM-IV (SCID) [18]. All SZ patients enrolled in COGS-2 met the DSM-IV diagnostic criteria for schizophrenia or schizoaffective disorder depressive type. Non-psychiatric comparison subjects were enrolled if they had:

- no current or past psychotic disorder
- a known biological family history
- no history of psychosis in a 1st degree relative
- no current Axis I mood disorder
- no Cluster-A Axis II disorder
- no current regular treatment with psychoactive medication

	Controls (NCS)	Patients (SZ)	p
Sample size	753	877	
Age Mean ± SD	38.63 ± 12.80	46.25 ± 11.23	<0.001
Education Mean ± SD	14.99 ± 2.20	12.63 ± 2.15	<0.001
Male	371 (49%)	616 (70%)	<0.001
Race	n (% full sample)	n (% full sample)	<0.001
Caucasian	438 (58%)	380 (43%)	
African American	159 (21%)	162 (18%)	
Other	156 (21%)	335 (38%)	
Smoker	84 (11%)	464 (53%)	<0.001
Age of Onset Mean ± SD		22.52 ± 7.23	
MMSE Mean ± SD	33.61 ± 1.69	31.12 ± 3.31	<0.001
SAPS Mean ± SD		6.88 ± 4.09	
SANS Mean ± SD		11.64 ± 5.36	

Supplementary Table 1. Clinical and demographic characteristics of the COGS-2 participants. Adapted from [17]. MMSE = Mini-Mental State Exam; SAPS = Scale for the Assessment of Positive Symptoms; SANS = Scale for the Assessment of Negative Symptoms.

The exclusion criteria (adapted from [18]) for the COGS-2 study are shown in Supplementary Table 2.

Exclusion Criteria	SZ	NCS
Adopted or family history unknown		X
Outside study age range of 18-65	X	X
Unable to understand consent due to language or competency	X	X
Physically unable to participate in testing of at least two endophenotypes	X	X
Previous endophenotype testing in the last 1 month	X	X
Previous neuropsychological testing in the last 3 months	X	X
Positive illicit drug or alcohol screen at the time of testing	X	X
Severe systemic illness that interferes with ability to be endophenotyped	X	X
Electroconvulsive treatment in the last 6 months	X	X
Alcohol or substance abuse in the past 1 month	X	X
Alcohol or substance dependence not in remission for 6 months	X	X
Significant head injury (loss of consciousness $>$ 15 min and/or neurological sequelae)	X	X
Neurological illness (e.g., seizures, stroke, Parkinson disease)	X	X
Less than one 1 month psychiatrically stable	X	
Estimated premorbid IQ $<$ 70 per Wide Range Achievement Test-Third Edition	X	X
History of psychosis in themselves or a family member (1st degree)		X
Current Axis I mood disorder		X
Cluster A personality disorder		X
Current treatment with antipsychotic agents		X
Current treatment with any psychoactive medication		X
Participated in COGS-1 testing	X	X
First-degree relative who has already participated in this study	X	X

Supplementary Table 2. Exclusion criteria for the COGS-2 testing. Adapted from [18].

4 Statistical Details of t-test Results

This section provides statistical details regarding the unpaired student's t-tests performed for Figs. 1–3 to identify time-windows where the group differences were statistically significant. Cohen's d effect sizes, t-statistic values, and degrees of freedom over all the time-windows are reported in Supplementary Figure 9. For ERP signals (deviant-minus-standard, deviant, and standard ERPs), an unpaired t-test was performed at each time-point (i.e. every ms) to identify time-points with significant group differences. For DDA signals, an unpaired t-test was performed at each time-window (i.e. every 10 ms). The false discovery rate (FDR) was adjusted using the Benjamini-Hochberg procedure [19].

In order to ensure that the group differences observed in the ERP and DDA signals are not mainly driven by the effects of age and gender, we repeated the above statistical analyses in

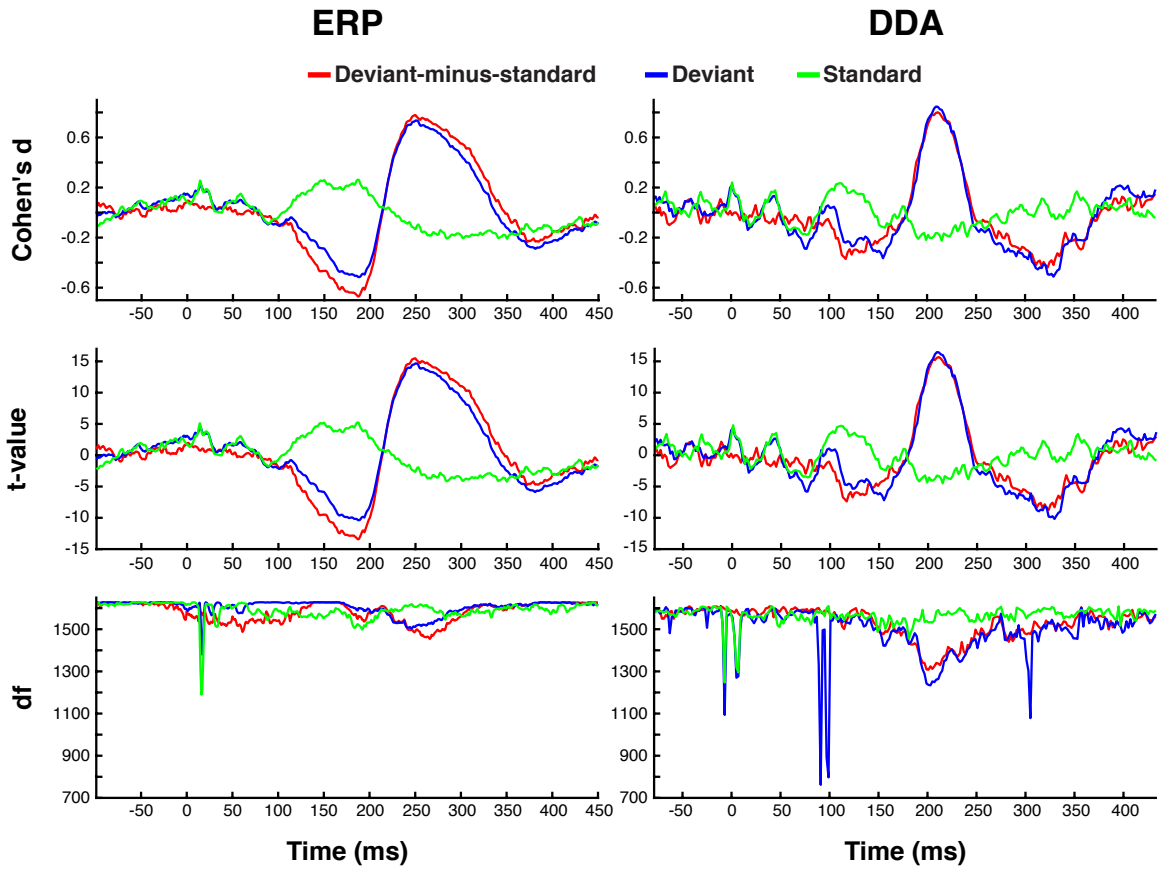

Supplementary Figure 9. Statistical details of the t-tests on ERP and DDA data. Effect sizes (Cohen's d), t-statstics, and degrees of freedom (df) for unpaired t-tests performed for ERP signals are shown in the left column. The same statistical measures are also plotted for the DDA time-series signals (right column).

subgroups that were matched in age and gender. We first divided the data into four subgroups based on the following four age ranges: 18–30 years old, 31–40 years old, 41–50 years old, and 51–65 years old. Within each age subgroup, we then sampled randomly to match the gender distribution. The following table summarizes the demographic characteristics of the four subgroups:

	18–30 years	31–40 years	41–50 years	51–65 years
Sample size	366	230	294	380
SZ	105 (29%)	120 (37.5%)	159 (54%)	260 (68%)
Male	183 (50%)	115 (50%)	147 (50%)	190 (50%)

Supplementary Table 3. Demographic characteristics of the four age subgroups.

t-statistic and Cohen's d values for the four age groups across all the time-windows are reported in Supplementary Figures 10 and 11, respectively.

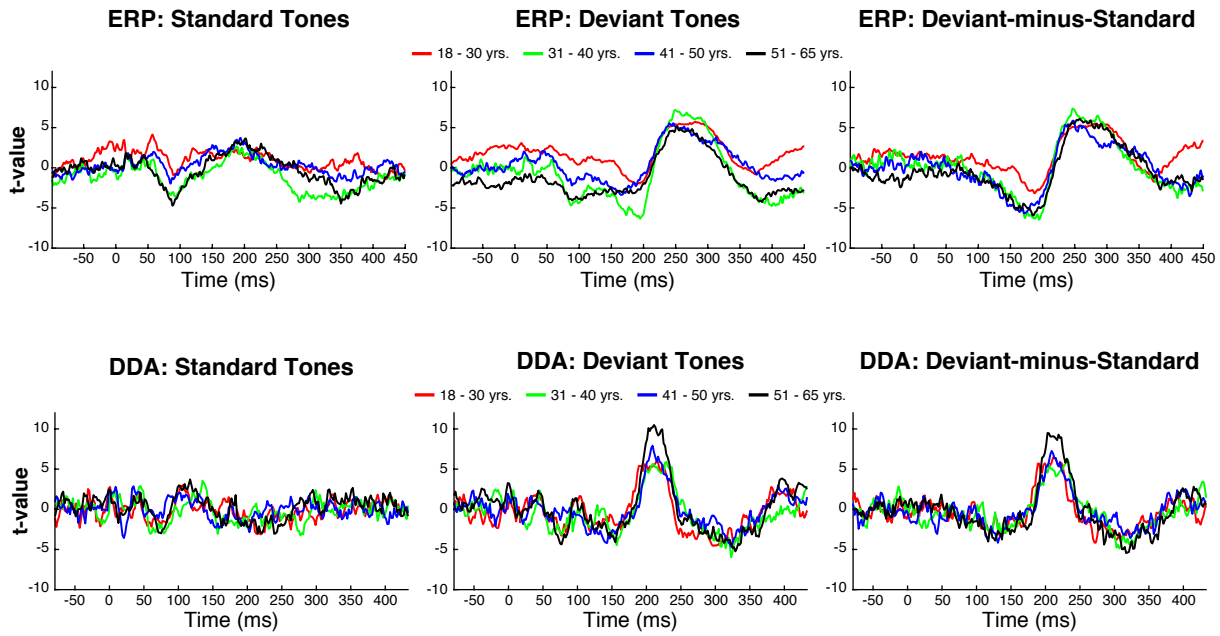

Supplementary Figure 10. t-statstics values from unpaired t-tests performed for ERP (top row) and DDA (bottom row) signals grouped by the four age bins are shown.

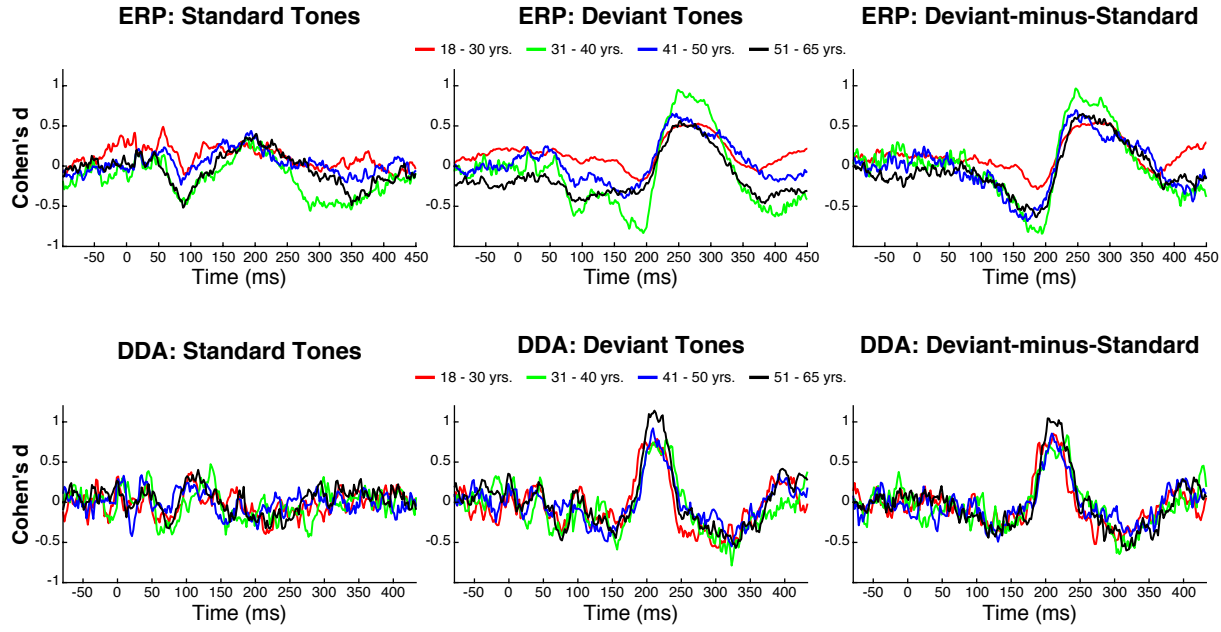

Supplementary Figure 11. Effect sizes (Cohen's d) values for ERP (top row) and DDA (bottom row) signals grouped by the four age bins are shown.

5 COGS Investigators

Gregory A. Light, Neal R. Swerdlow, Michael L. Thomas, Michael F. Green, Tiffany A. Greenwood, Raquel E. Gur, Ruben C. Gur, Laura C. Lazzeroni, Keith H. Nuechterlein, Allen D. Radant, Larry J. Seidman, Richard F. Sharp, Larry J. Siever, Jeremy M. Silverman, Joyce Sprock, William S. Stone, Catherine A. Sugar, Debby W. Tsuang, Ming T. Tsuang, Bruce I. Turetsky, David L. Braff

References

1. M. Kremliovsky, J. Kadtke, Using delay differential equations as dynamical classifiers, AIP Conference Proceedings 411 (1997) 57.

2. J. Kadtke, M. Kremliovsky, Estimating statistics for detecting determinism using global dynamical models, Phys. Lett. A 229(2) (1997) 97.

3. C. Lainscsek, P. Rowat, L. Schettino, D. Lee, D. Song, C. Letellier, H. Poizner, Finger tapping movements of Parkinson's disease patients automatically rated using nonlinear delay differential equations, Chaos 22 (2012) 013119.

4. C. Lainscsek, T. Sejnowski, Electrocardiogram classification using delay differential equations, Chaos 23(2) (2013) 023132.

5. C. Lainscsek, T. Sejnowski, Delay differential analysis of time series, Neural Computation 27 (3) (2015) 594–614.

6. Whitney, Differentiable manifolds, Ann. Math. 37 (1936) 645–680.

7. N. H. Packard, J. P. Crutchfield, J. D. Farmer, R. S. Shaw, Geometry from a time series, Phys. Rev. Lett. 45 (1980) 712.

8. F. Takens, Detecting strange attractors in turbulence, in: D. A. Rand, L.-S. Young (Eds.), Dynamical Systems and Turbulence, Warwick 1980, Vol. 898 of Lecture Notes in Mathematics, Springer Berlin/Heidelberg, 1981, pp. 366–381.

9. T. Sauer, J. A. Yorke, M. Casdagli, Embedology, Journal of Statistical Physics 65 (1991) 579.

10. C. E. Falbo, Analytic and numerical solutions to the delay differential equation $y'(t) = \alpha y(t - \delta)$, in: Joint meeting of the Northern and Southern California sections of the MAA, San Luis Obispo, CA, 1995.

11. C. Lainscsek, Nonuniqueness of global modeling and time scaling, Phys. Rev. E 84 (2011) 046205.

12. C. Lainscsek, A class of lorenz-like systems, Chaos 22 (2012) 013126.

13. E. Miletics, G. Molnárka, Implicit extension of Taylor series method with numerical derivatives for initial value problems, Comput. Math. Appl. 50 (7) (2005) 1167–1177.

14. L. Boltzmann, Vorlesungen über Gastheorie, Leipzig, J.A. Barth, 1898, ("Ergoden" in chapter III, 32).

15. R. Kohavi, A study of cross-validation and bootstrap for accuracy estimation and model selection, in: Proceedings of the 14th international joint conference on Artificial Intelligence - Volume 2, IJCAI'95, Morgan Kaufmann Publishers Inc., 1995, pp. 1137–1143.

16. D. Hand, R. Till, A simple generation of the area under the roc curve for multiple class classification problems, Machine Learning (45) (2001) 171–186.

17. G. A. Light, N. R. Swerdlow, M. L. Thomas, M. E. Calkins, M. F. Green, T. A. Greenwood, R. E. Gur, R. C. Gur, L. C. Lazzeroni, K. H. Nuechterlein, M. Pela, A. D. Radant, L. J. Seidman, R. F. Sharp, L. J. Siever, J. M. Silverman, J. Sprock, W. S. Stone, C. A. Sugar, D. W. Tsuang, M. T. Tsuang, D. L. Braff, B. I. Turetsky, Validation of mismatch negativity and P3a for use in multi-site studies of schizophrenia: Characterization of demographic, clinical, cognitive, and functional correlates in COGS-2, Schizophrenia Research 163 (1) (2015) 63 – 72.

18. N. R. Swerdlow, R. E. Gur, D. L. Braff, Consortium on the Genetics of Schizophrenia (COGS) assessment of endophenotypes for schizophrenia: An introduction to this special issue of schizophrenia research, Schizophrenia Research 163 (1) (2015) 9 – 16.

19. Y. Benjamini, Y. Hochberg, Controlling the false discovery rate: A practical and powerful approach to multiple testing, Journal of the Royal Statistical Society. Series B (Methodological) 57 (1) (1995) 289–300.